Chemical Reactions in CF_2Cl_2/Water (Ice) Films Induced by X-ray Radiation

C. C. Perry,[†] G. M. Wolfe,[†] A. J. Wagner,[†] J. Torres,[†] N. S. Faradzhev,[‡] T. E. Madey,[‡] and D. H. Fairbrother*[,†]

Department of Chemistry, Johns Hopkins University, 3400 N. Charles Street, Baltimore, Maryland 21218, and Laboratory for Surface Modification and Department of Physics and Astronomy, Rutgers, The State University of New Jersey, Piscataway, New Jersey 08854-8019

Received: April 25, 2003; In Final Form: July 3, 2003

The chemical reactions initiated by high-energy radiation (Mg or Al K_α X-rays) in amorphous CF_2Cl_2/H_2O(ice) films have been studied using a combination of reflection absorption infrared spectroscopy (RAIRS), X-ray photoelectron spectroscopy (XPS), and temperature programmed desorption (TPD). Following deposition, the structure of the CF_2Cl_2/H_2O(ice) film resembles an amorphous ice phase having CF_2Cl_2 molecules caged within the film, and a smaller number of CF_2Cl_2 molecules adsorbed on the ice surface. X-ray irradiation produces a broad distribution of low-energy secondary electrons whose interactions with CF_2Cl_2/H_2O(ice) films are associated with the production of H_3O^+, CO_2, and COF_2 (carbonyl fluoride) as detected by RAIRS. COF_2 is identified as an intermediate species whose electron-stimulated decomposition leads to CO_2 production. The product partitioning is dependent on the film's initial composition; in water rich films, CO_2 and COF_2 production is favored, whereas a more thermally stable, partially halogenated polymeric CF_xCl_y film is detected by XPS in CF_2Cl_2 rich films. Chloride and fluoride anions are also produced and solvated (trapped) within the ice film. During the early stages of X-ray irradiation, the dominance of Cl^- anions formed in the film by reaction with low-energy secondary electrons is consistent with the suggestion that C−Cl bond cleavage of CF_2Cl_2 via dissociative electron attachment ($CF_2Cl_2 + e^- \rightarrow \cdot CF_2Cl + Cl^-$) is the dominant initial process.

1. Introduction

Chlorofluorocarbons (CFCs) such as CF_2Cl_2 (Freon-12 or CFC-12), once widely used as refrigerants and propellants, are susceptible to UV photodissociation in the stratosphere.[1] The resultant Cl atoms generated during the photolysis process participate in the ClO_x catalytic cycle and have been identified with the ozone layer depletion in the Antarctic spring.[2] This ozone depletion in the Antarctic stratosphere has been linked to the heterogeneous chlorine chemistry that occurs on polar stratospheric clouds (PSCs) at temperatures below ∼200 K.[3]

In contrast to studies of photochemical processes relevant to the stratosphere, the interaction of high-energy radiation with atmospheric gases such as CFCs is poorly understood. The biggest source of high-energy radiation in the stratosphere is in the form of cosmic rays[4,5] (high-energy particles) from space. Although cosmic rays are associated with radiation in excess of thousands of electronvolts, the primary result from the interaction of such high-energy radiation with matter involves the production of a cascade of low-energy secondary electrons. For these low-energy electrons (E_{kin} < 10 eV) in the energy range below the threshold for dipolar dissociation (DD) (∼15 eV),[6,7] dissociative electron attachment (DEA) to molecules has been recognized as a major mechanism leading to stable anion and free-radical formation.[8,9] DEA consists of resonant electron capture into a relatively short-lived molecular ion state, which is dissociative in the Franck−Condon region. When the lifetime of this state is similar to, or longer than, the vibrational period of nuclear motion, the transient anion can dissociate into neutral and anionic fragments if at least one of these has a positive electron affinity.[8,9]

Electron-stimulated reactions in atmospheric chemistry have largely been ignored because of the low free electron density in the stratosphere.[10] Recently, however, there has been an increased interest in the role of electron-stimulated reactions associated with chlorofluorocarbons as a result of studies indicating that negative ion yields (Cl^-, F^-) from CF_2Cl_2 coadsorbed with polar dielectric molecules (water and ammonia) on a metal surface are several orders of magnitude higher than for CF_2Cl_2 adsorbed alone.[11−14] In addition, Lu and Sanche[13] have reported that CF_2Cl_2 molecules adsorbed on top of H_2O and NH_3 surfaces exhibit giant enhancements in the charge trapping coefficient that they attributed to increases in the DEA cross-section.[12,13] On the basis of these observations, Lu and Sanche[15] proposed that CFCs adsorbed on PSCs could also be destroyed via the DEA process to produce Cl^- that becomes involved in the catalytic destruction of ozone. The relative importance of this mechanism to stratospheric ozone depletion, however, is still a matter of debate.[16−19]

The interaction of gas-phase CF_2Cl_2 with low-energy electrons (∼0 eV) leads predominantly to C−Cl bond scission to produce Cl^- and a trihalomethyl radical ($\cdot CF_2Cl$).[9,20−22]

$$CCl_2F_2 + e^- \rightarrow \cdot CF_2\,Cl + Cl^- \qquad (1)$$

Under atmospheric conditions, the subsequent reactivity of carbon-containing radicals can involve oxygen-containing species leading to the formation of new, stratospherically important species such as carbon dioxide and/or the carbonyl dihalides

* Corresponding author. E-mail address: howardf@jhu.edu.
† Johns Hopkins University.
‡ Rutgers, The State University of New Jersey.

10.1021/jp035129k CCC: $25.00
Published on Web 10/28/2003

($COCl_2$, COF_2, or COFCl) that themselves may undergo UV photodissociation, yielding haloformyl radicals XCO and halogen atoms.[23] In comparison, the interaction of low-energy electrons or high-energy (ionizing) radiation with water(ice) produces hydroxyl radicals (OH), hydrogen atoms (H), and hydrated electrons (e^-) as the dominant reaction intermediates.[24] Neutral gas-phase products have been detected during the interaction of <200 eV electrons with amorphous D_2O (D-ice) including atomic D and O, as well as D_2 and O_2[25−31] although a number of charged species including H^+ [32] and $H^-(D^-)$[33] have also been observed.

In previous studies in our laboratory, we have investigated the effect of electron beam irradiation on carbon tetrachloride/water(ice) films where CO_2, CO, and HCl were identified as the neutral gas-phase products whereas $COCl_2$, C_2Cl_4, and H_3O^+ as well as chloride ions were produced in the film.[34,35] In dilute films where the CCl_4:H_2O ratio is low, CO_2 is the dominant carbon-containing fragment, whereas in films more concentrated with CCl_4, carbon−carbon coupling reactions became increasingly prevalent.

In the present study, a conventional Mg/Al X-ray source is employed to model the effects of high-energy radiation on CF_2Cl_2/H_2O(ice) films. The focus of this investigation is to explore the chemical reactions associated with carbon-containing fragments that are initiated in CF_2Cl_2/H_2O(ice) films by high-energy radiation, motivated by the importance of both CF_2Cl_2 and H_2O in the stratosphere, the latter existing in the form of polar stratospheric clouds (PSCs). In addition, the effect of X-ray irradiation on organohalides adsorbed in ice films has implications for electron beam[36] and plasma[37,38] remediation strategies. In CF_2Cl_2/H_2O(ice) films exposed to X-ray radiation, the molecular species CO_2 and COF_2 are produced, along with hydroxonium and halide (Cl^- and F^-) ions that are effectively solvated within the ice film. There is negligible loss of total F and Cl during X-ray irradiation. RAIRS and XPS measurements also reveal that the product distribution is dependent on the film's initial composition; in water-rich films ($CF_2Cl_2/H_2O \leq 0.1$), RAIRS experiments showed that CO_2 and COF_2 production is favored. In CF_2Cl_2 rich films ($CF_2Cl_2/H_2O \gg 0.1$), however, XPS measurements indicate that a thermally stable partially halogenated polymeric CF_xCl_y film is produced due to carbon−carbon coupling reactions.

2. Experimental Section

Experiments were carried out in three separate ultrahigh-vacuum systems. The first system (chamber 1) was equipped with capabilities for X-ray photoelectron spectroscopy (XPS) and mass spectrometry (MS) (Stanford Research Systems (RGA200) or a Balzers 200 amu Prisma) as described previously.[39] The second system (chamber 2) was an integrated two-chamber design equipped with capabilities for reflection−absorption infrared spectroscopy (RAIRS), MS, and XPS described elsewhere.[34,40] A base pressure of $\approx 2 \times 10^{-9}$ Torr was maintained during experiments in chambers 1 and 2. The third system (chamber 3) consisted of a chamber (base pressure $\approx 5 \times 10^{-11}$ Torr) equipped with multiple surface analytical capabilities, including Auger electron spectroscopy (AES) and temperature programmed desorption (TPD).[41]

Film Preparation and Sample Cooling. In both XPS systems (chambers 1 and 2), high-purity dichlorodifluoromethane CF_2Cl_2 (Matheson, 99.995%) was stored in a metal vacuum cylinder whereas H_2O (Millipore, deionized) was stored in a glass vacuum bulb; both were attached to a gas manifold via separate lines. In chambers 1 and 2, CF_2Cl_2/H_2O mixtures were deposited on Au substrates cooled to ≈100 K, as described elsewhere.[34,35] In each chamber, the film was generated by co-deposition of the CF_2Cl_2 and H_2O components of the gas mixture while the gas purity during dosing was monitored by mass spectrometry at chamber pressures ranging between 10^{-6} and 10^{-7} Torr. In chamber 3, both H_2O and CF_2Cl_2 were stored in separate metal vacuum cylinders. In chamber 3, the sample was a Ru(0001) crystal attached to a closed-cycle helium refrigerator, enabling sample cooling to 25 K. CF_2Cl_2/H_2O films were deposited via a doser capped with a microcapillary array.

It should be noted that there was evidence of Au halide formation (AuCl/AuF) near the Au interface during X-ray irradiation. As a result of this, all XP spectra recorded in this investigation were obtained from films where the substrate Au signal was less than 5% of its initial value, ensuring that changes within the C 1s, F 1s, Cl 2p, and O 1s regions were due to chemical transformations within the film rather than at the film/substrate interface. One component of this study involved the effect of the film's initial chemical composition on the reaction kinetics and product partitioning. The average chemical composition of the film was determined from XPS (Chamber 1 and 2) and TPD (Chamber 3), defined as dilute for initial CF_2Cl_2:H_2O ratios <0.1 and concentrated if the CF_2Cl_2:H_2O ratio was initially ≥0.3.

XPS Experiments (Chamber 1). CF_2Cl_2/H_2O(ice) films were condensed onto an Ar^+ sputter-cleaned polycrystalline gold substrate (99.95%, Goodfellow) (size: ∼1 cm^2) that was mounted on a tantalum sample holder attached to a ceramic feed-through coupled to an UHV sample manipulator. A sample temperature of ≈100 K was maintained by passing liquid nitrogen into a hollow stainless steel rod connected to the ceramic-feedthrough as described previously.[39] The temperature of the Au substrate was monitored via a chromel−alumel thermocouple directly attached to the Ta sample holder. X-ray irradiation and XPS analysis of the CF_2Cl_2/H_2O(ice) films were done using the output from a Mg Kα anode (1253.6 eV) operating at 300 W and 15 kV, with a 45° takeoff angle relative to the surface normal. All elemental XP spectra were calibrated on either the Cl^- $2p_{3/2}$ peak at 198 eV or the C−Cl $2p_{3/2}$ peak at 201 eV within the Cl 2p region.[42]

In chamber 1, the composition and thickness of the CF_2Cl_2/H_2O adsorbed films after deposition were monitored by XPS. Each film's concentration was determined using the ratio of the F 1s and O 1s XPS areas of the initial film, accounting for stoichiometry and elemental sensitivity factors.[43] Typical film thicknesses of ∼60−70 Å were calculated, using the attenuation of the Au 4f photoelectrons in water (ice).[44]

RAIRS Experiments (Chamber 2). RAIR spectra were recorded with a Mattson Infinity series FTIR spectrometer equipped with external beam capabilities, a narrow-band mercury−cadmium-telluride (MCT) detector (700−4000 cm^{-1}) and a quadrupole mass spectrometer (QMS). All spectra were taken with a resolution of 4 cm^{-1} by summing 500 scans and were referenced to the Au surface at ≈100 K before CF_2Cl_2/H_2O adsorption. XPS analysis and X-ray irradiation were carried out using either the Mg or Al anode of a commercial X-ray gun as described previously.[34]

In the RAIRS experiments, XPS analysis following CF_2Cl_2/H_2O film deposition revealed that the Au 4f substrate signal (<1%) could not be detected. This indicated the adsorption of a thick (>120 Å) film, on the basis of the inelastic mean free path of ∼1200 eV electrons in water.[44] The growth of a thick film was done to improve the signal-to-noise of IR bands associated with product species generated by X-ray irradiation

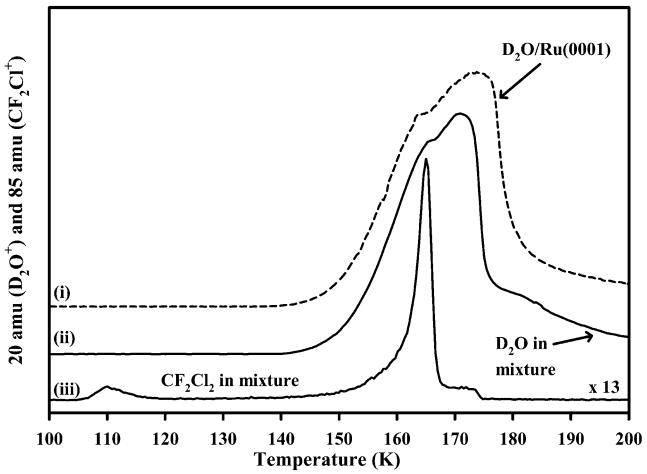

Figure 1. TPD spectra for both a pure D_2O(ice) film and a CF_2Cl_2/D_2O mixed film (CF_2Cl_2:D_2O ratio $\approx$ 0.04): (i) $m/q = 20$ for a pure D_2O(ice) film (shown as a dashed line); (ii) $m/q = 20$ for water (D_2O) in CF_2Cl_2/D_2O film; (iii) $m/q = 85$ $(CF_2Cl)^+$ for CF_2Cl_2 signal in the CF_2Cl_2/D_2O film. (Mixed film data, (ii) and (iii), are shown as solid lines). The heating rate is $\approx$ 1 K/s.

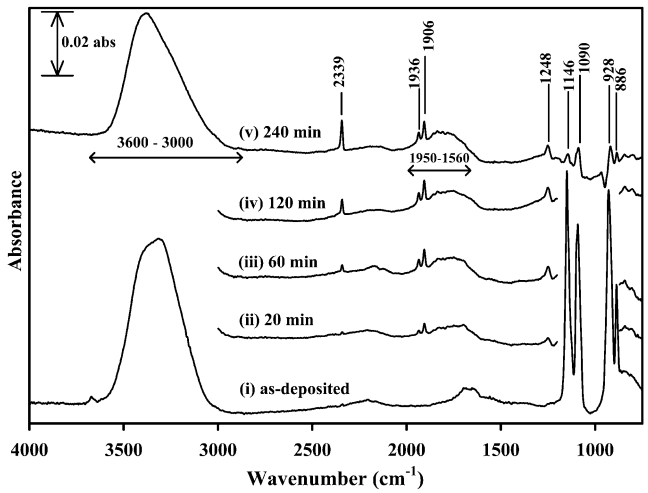

Figure 2. Variations in the RAIR spectra of a CF_2Cl_2/H_2O (CF_2Cl_2:H_2O $\approx$ 0.28) film as a function of X-ray exposure: (i) as-deposited; (ii) 20 min; (iii) 60 min; (iv) 120 min; (v) 240 min. All RAIRS spectra were referenced to the clean cooled Au substrate. Peak assignments are given in Table 1.

and to ensure that observed species were a result of reactions within the CF_2Cl_2/H_2O(ice) film.

Thermal Desorption Experiments (Chamber 3). Thermal desorption experiments were performed on a Ru(0001) sample (size $\sim$1 cm^2) mounted on an XYZ-rotary manipulator. A tungsten filament located behind the sample allowed electron bombardment heating to 1600 K. The surface was cleaned by heating to $\sim$1600 K, as well as by occasional Ar^+ sputtering and oxygen heat treatments. Surface cleanliness was monitored by Auger electron spectroscopy (AES) and low-energy electron diffraction (LEED). A base pressure of $\sim 5 \times 10^{-11}$ Torr was maintained during these experiments.

After CF_2Cl_2/H_2O(ice) films were condensed at 25 K onto the Ru(0001) sample, the coverages and adsorption/desorption kinetics were measured using TPD. For TPD, the surface was heated (heating rate $\sim$1 K s^{-1}) via radiation from a hot W filament located behind the sample. Gases desorbed via TPD were detected using a QMS (UTI, model 100C) located 5 cm from the sample. The sample was biased at -200 V during TPD to prevent electron-induced damage of the film from electrons in the QMS ionization source.

In the TPD system (chamber 3), the thickness and composition of the adsorbed films were determined from the area of the monolayer peaks obtained for CF_2Cl_2 and H_2O dosed on Ru(0001). These areas were then used as reference points for calculating the total coverage and partial concentrations of the components within CF_2Cl_2/H_2O films.

3. Results

Figure 1(i) shows the TPD spectra of water (D_2O) from a pure water(ice) film. The thickness of the film is $\sim$10 monolayers (ML) corresponding to 10 hydrogen-bonded bilayers.[45,46] Pure D_2O (20 amu/D_2O^+) exhibits a shoulder at $\approx$165 K in addition to a peak due to the sublimation of the condensed ice phase at $\approx$170 K. This shoulder is observed in previous desorption studies and is assigned to an irreversible phase transition from the amorphous to the crystalline phase.[47] Parts ii and iii of Figure 1 correspond to the peaks associated with water (20 amu/D_2O^+) and CF_2Cl_2 (85 amu/CF_2Cl^+) desorption from a dilute coadsorbed CF_2Cl_2/water film (CF_2Cl_2:D_2O ratio $\approx$0.04). Figure 1(ii) exhibits two features centered at $\approx$165 and $\approx$170 K, coincident with the amorphous/crystalline phase transition and the sublimation of crystalline D_2O, respectively. Figure 1(iii) illustrates that the CF_2Cl_2 signal exhibits distinct desorption peaks centered at $\approx$110 K, $\approx$165 K and a small shoulder at $\approx$170 K.

Figure 2 shows the RAIR spectra of a CF_2Cl_2/H_2O film (CF_2Cl_2:H_2O $\approx$ 0.28) as a function of X-ray irradiation time. The initial CF_2Cl_2/H_2O film after adsorption consists of IR bands associated with the O$-$H stretching mode of H_2O (3000$-$3600 cm^{-1}) and the in-plane deformation mode (1600$-$1700 cm^{-1}) (Figure 2(i)).[48,49] The peak around 3700 cm^{-1} is assigned to free O$-$H groups at the film/vacuum interface of an amorphous ice surface.[50] The IR peaks at 1146 and 1090 cm^{-1} are identified with the C$-$F symmetric and asymmetric stretches of CF_2Cl_2,[51] whereas the peaks at 928 and 886 cm^{-1} comprise a Fermi doublet, consisting of the ν_{as}(CCl) and δ(C$-$F) + γ(C$-$F) modes of CF_2Cl_2, respectively.[51,52]

Figure 2(ii)$-$(v) shows that upon X-ray irradiation, the IR bands associated with the CF_2Cl_2 molecules as well as the free OH species decrease, coupled with the appearance of new peaks at 2339, 1936, 1906, and 1248 cm^{-1}. The 2339 cm^{-1} peak position is diagnostic of the presence of CO_2 whereas the peaks at 1936 and 1906 cm^{-1} are assigned to a Fermi doublet, composed of the ν_2(CO) and $2\nu_1$(C$-$F) stretches of carbonyl difluoride (COF_2), respectively.[51,53,54] Similarly, the 1248 cm^{-1} peak is assigned to the ν(C$-$F) stretch of COF_2. The idea that the bands at 1906, 1936, and 1248 cm^{-1} are all associated with a common species is supported by the fact that the ratio of these three peak areas remained constant over the course of X-ray irradiation. There was no evidence of the Fermi doublet (ν_1(CO) and (ν_2(CF) + ν_3(CCl))) and ν_2(CF) stretching modes associated with carbonyl chloride fluoride (COFCl) expected at 1876, 1850, and 1095 cm^{-1}, respectively.[51] Similarly, there was no evidence of phosgene ($COCl_2$) production, as evidenced by the absence of the ν(CO) stretch at 1798 cm^{-1}.[34] In addition to the sharp new IR peaks associated with discrete molecular species, a broad IR band between 1950 and 1560 cm^{-1} was observed during X-ray irradiation. These new features are assigned to the antisymmetric bending mode of the hydroxonium ion (H_3O^+) in an amorphous ice film.[55] The production of H_3O^+ species is also consistent with the broadening and red shifting of the ν(OH) stretching mode, which has also been observed in previous studies during HBr and HCl reactions with ice films.[56,57]

TABLE 1: Observed Frequencies in the Infrared Spectrum of CF_2Cl_2/H_2O Ice Films

frequencies (cm^{-1})	assignment	mode description[a]
3000−3600	H_2O	ν(O−H) str
2339	CO_2	ν(C═O) str
1936	COF_2	ν_1(CO) str
1906	COF_2	$2\nu_2$(C−F) str (FR)
1560−1950	H_3O^+	$\delta_a(H_3O^+)$ def
1600−1700	H_2O	$\delta(H_2O)$ def
1180−1250	H_3O^+	$\delta_s(H_3O^+)$ def
1248	COF_2	ν_4(C−F) str
1146	CF_2Cl_2	ν_{as}(C−F) str
1090	CF_2Cl_2	ν_s(C−F) str
928	CF_2Cl_2	ν_{as}(C−Cl) str
886	CF_2Cl_2	δ(C−F) + γ(C−F) (FR)

[a] FR, Fermi Resonance; γ, out-of-plane deformation; ν_s, symmetric stretch; δ, in-plane deformation; ν_{as}, asymmetric stretch.

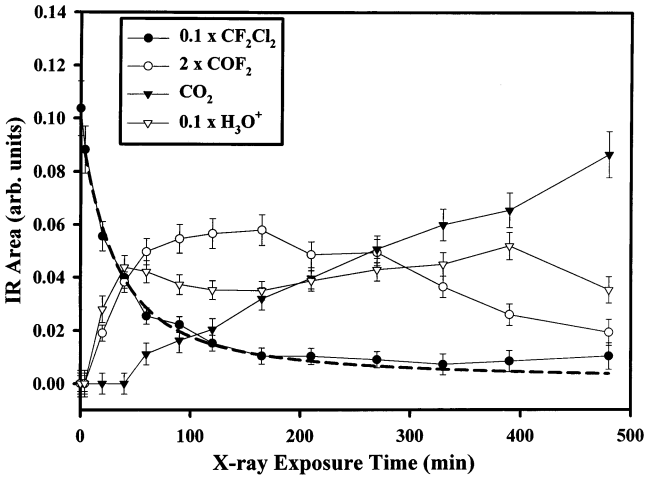

Figure 3. Variation in the integrated IR areas of CF_2Cl_2 (●) (sum of the 1146 and 1090 cm^{-1} peaks), COF_2 (○) (sum of the 1936 and 1906 cm^{-1} peak areas), CO_2 (▼) (2339 cm^{-1}), and H_3O^+ (▽) (1700−1500 cm^{-1}) bands during X-ray exposure of a CF_2Cl_2/H_2O film (CF_2Cl_2:$H_2O \approx 0.11$). The dashed line represents the best-fit first-order decay calculated for the loss of CF_2Cl_2 that incorporates the nonuniform spatial intensity profile of the X-ray beam.

Peak assignments for all of the IR bands observed in the present study are given in Table 1.

For a different CF_2Cl_2/H_2O(ice) film (CF_2Cl_2:$H_2O \approx 0.11$), the variation in the integrated IR areas of the CF_2Cl_2 peaks (1146 and 1090 cm^{-1}), the COF_2 Fermi doublet (1936 and 1906 cm^{-1}), the CO_2 peak (2339 cm^{-1}), and the H_3O^+ band (1700−1500 cm^{-1}) as a function of prolonged X-ray exposure were measured. Results from this experiment are shown in Figure 3. During the initial period of X-ray exposure (<50 min), changes in the RAIR spectra are dominated by the decrease in the CF_2Cl_2 area accompanied by the appearance of COF_2 and H_3O^+. In contrast, the CO_2 peak is absent with a short induction period for X-ray exposures (<40 min) before increasing roughly linearly for increasing X-ray irradiation times. Figure 3 also shows that the area of the COF_2 peak passes through a maximum and decreases upon prolonged X-ray exposure (180 min). The dashed line in Figure 3 is a best-fit first-order decay profile for the loss of CF_2Cl_2 from the film, which incorporates the nonuniform spatial intensity profile anticipated for the X-ray source.[58,59]

Figure 4 shows RAIR spectra illustrating the effect of the film's initial CF_2Cl_2/H_2O composition on the product distribution after a fixed period of X-ray exposure (40 min). In these experiments, the total amount of CF_2Cl_2 within the film was held constant on the basis of the integrated area of the initial

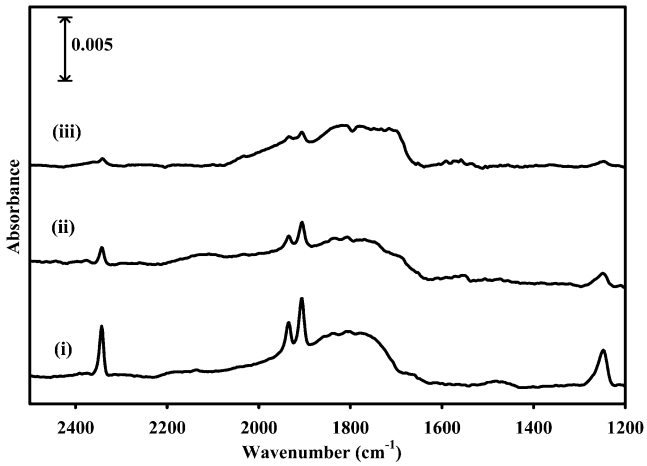

Figure 4. Variation in the IR spectra for (i) CF_2Cl_2:$H_2O \approx 0.09$, (ii) CF_2Cl_2:$H_2O \approx 0.19$, and (iii) CF_2Cl_2:$H_2O \approx 0.26$ films, after 40 min of X-ray irradiation. All spectra in Figure 4 are difference spectra referenced to the initial CF_2Cl_2/H_2O film. Peak assignments are given in Table 1.

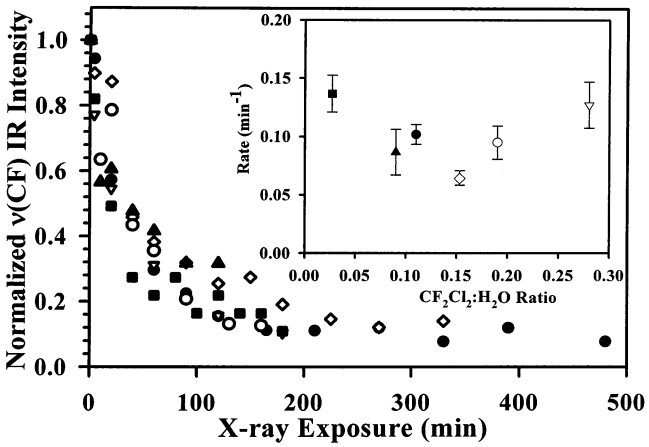

Figure 5. Plot of the ν(CF) bands intensity for a series of CF_2Cl_2/H_2O films of different initial chemical composition as a function of X-ray exposure: CF_2Cl_2:H_2O = 0.09 (▲), CF_2Cl_2:H_2O = 0.28 (▽), CF_2Cl_2:H_2O = 0.03 (■), CF_2Cl_2:H_2O = 0.19 (○), CF_2Cl_2:H_2O = 0.11 (●), and CF_2Cl_2:H_2O = 0.15 (◇). In each case, the ν(CF) band area has been normalized to the value obtained for the initial film prior to X-ray irradiation. The inset shows the rate of CF_2Cl_2 loss calculated for the films in Figure 5.

IR peaks at 1146 and 1090 cm^{-1} whereas the relative amount of the H_2O (measured by the integrated area of the O−H stretching mode) was varied. This approach was employed to ensure that the total amount of initial carbon-containing species (i.e., CF_2Cl_2) in the films was constant whereas the CF_2Cl_2:H_2O ratio varied. Figure 4 shows that the concentration of CO_2 and COF_2 produced is dependent upon the film's initial CF_2Cl_2:H_2O ratio, being greatest for more H_2O rich films.

In contrast to Figure 4, which shows the effect of the film's initial chemical composition on the concentrations of COF_2 and CO_2 after a fixed period of X-ray irradiation, Figure 5 shows the influence of the film's initial chemical composition on the kinetics of the parent CF_2Cl_2 loss. Figure 5 is a plot of the loss of CF_2Cl_2 parent measured by the decrease in the integrated IR area of the ν(CF) bands as a function of X-ray irradiation for six films that possess different initial CF_2Cl_2:H_2O ratios. In each case, the amount of CF_2Cl_2 present in the film was determined from the integrated intensity of the ν(CF) bands (1090 and 1146 cm^{-1}) normalized to the initial ν(CF) integrated intensity. Four of the films have an identical initial H_2O content (measured by

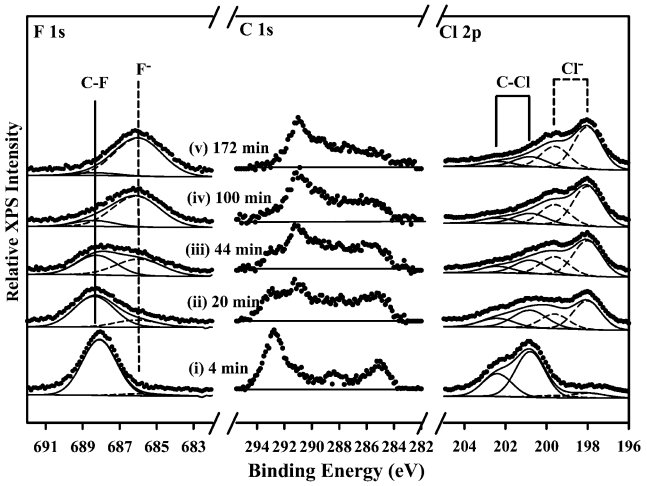

Figure 6. Variation of the F 1s, C 1s, and Cl 2p XPS regions of a CF_2Cl_2/H_2O film (CF_2Cl_2:$H_2O \approx 0.04$) as a function of X-ray exposure time: (i) 4 min; (ii) 20 min; (iii) 44 min; (iv) 100 min; (v) 172 min. The fits in the F 1s and Cl 2p regions contain solid lines for the C−F and C−Cl species and dotted lines for the F^- and Cl^- ions, respectively.

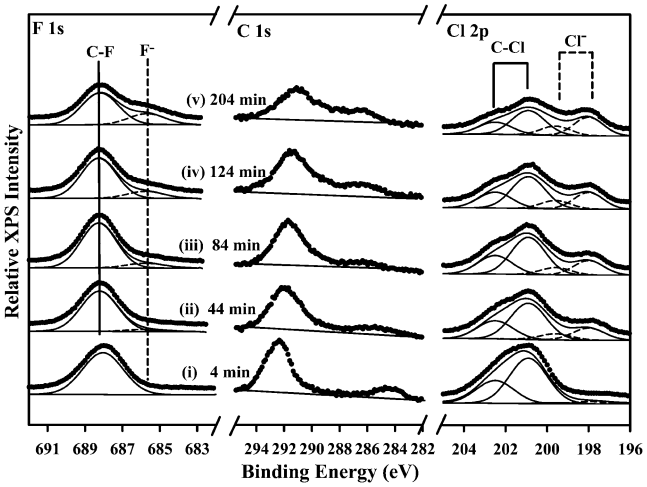

Figure 7. Variation of the F 1s, C 1s, and Cl 2p XPS regions of a CF_2Cl_2/H_2O film (CF_2Cl_2:$H_2O \approx 0.28$) as a function of X-ray exposure time: (i) 4 min; (ii) 44 min; (iii) 84 min; (iv) 124 min; (v) 204 min. The fits in the F 1s and Cl 2p regions contain solid lines for the native C−F and C−Cl species and dotted lines for the F^- and Cl^- species, respectively.

the area of $\nu(OH)_{t=0}$) and two have a constant CF_2Cl_2 content ($\nu(CF)_{t=0}$). Inspection of Figure 5 reveals that the rate of CF_2Cl_2 loss is not strongly dependent upon the film's initial chemical composition (shown explicitly in the inset for the calculated first-order rate constant associated with the loss of CF_2Cl_2 as a function of the film's initial chemical composition).

Figure 6 shows the evolution of the F 1s, C 1s (baseline corrected) and Cl 2p XPS data for a CF_2Cl_2/H_2O film (CF_2Cl_2:$H_2O \approx 0.04$) as a function of X-ray irradiation time. The XPS peaks associated with CF_2Cl_2 are the single C−F peak in the F 1s region (≈688 eV) and a C−Cl $2p_{3/2}/2p_{1/2}$ doublet in the Cl 2p region, with the $2p_{3/2}$ peak located at ≈201 eV[42] (Figure 6(i)). In addition, the C 1s peak associated with the native CF_2Cl_2 species can be observed at ≈293 eV, whereas the peak at 285 eV is assigned to adventitious carbon contamination. During X-ray irradiation, changes are observed in the F 1s, Cl 2p, and C 1s regions. At short irradiation times (<20 min), the Cl 2p XPS spectral envelope broadens to lower binding energies, requiring the inclusion of a new $2p_{3/2}/2p_{1/2}$ doublet with a $2p_{3/2}$ peak at ≈198 eV, consistent with the formation of chloride ions.[42] Over the corresponding time scale in the C 1s region, a new peak appears at ≈291 eV at the expense of the native CF_2Cl_2 peak. RAIRS data indicate that in dilute films (Figure 6(i)) where the CF_2Cl_2:H_2O ratio is low, CO_2 is expected to be the dominant carbon-containing molecular species in the film after prolonged X-ray exposures, enabling us to identify the peak at ≈291 eV as CO_2. This peak position also coincides with results obtained during control experiments involving CO_2 deposition onto ice films. Although the production of chloride ions is dominant during the initial stages of irradiation, for longer X-ray exposures (>20 min) the appearance of fluoride ions becomes increasingly apparent in the F 1s region; this is evidenced by the broadening of the F 1s region to lower binding energies requiring the inclusion of a new peak centered at ≈686 eV;[42] see Figure 6(iii)−(v). Figure 6 also shows that for prolonged X-ray exposures, the XPS peaks associated with chloride and fluoride ions in the Cl 2p and F 1s regions become the dominant features relative to the C−Cl and C−F species (Figure 6(ii)−-(v)).

The evolution of the F 1s, C 1s, and Cl 2p XPS regions of a more concentrated CF_2Cl_2/H_2O (CF_2Cl_2:$H_2O \approx 0.28$) film as a function of X-ray irradiation are shown in Figure 7. Although fluoride and chloride ions are both produced during the

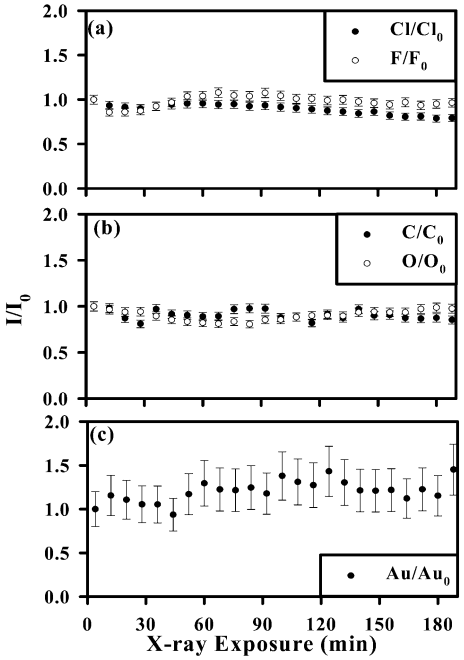

Figure 8. Variation in the C 1s, Cl 2p, F 1s, O 1s, and Au 4f XP regions (normalized to their initial values) as a function of X-ray exposure: (a) chlorine (●, Cl/Cl_0) and fluorine (○, F/F_0); (b) carbon (●, C/C_0), oxygen (○, O/O_0); (c) gold (●, Au/Au_0).

irradiation process, a comparison of Figures 6 and 7 shows that for the same X-ray exposure times, the relative extent of chloride and fluoride ion production is reduced in the more concentrated film (cf. Figures 6(iii) and 7(ii); 44 min). Figure 8 shows elemental plots of the integrated C 1s, Cl 2p, F 1s, O 1s, and Au 4f XPS signals normalized to the initial elemental areas for the CF_2Cl_2/H_2O film shown in Figure 7 as a function of X-ray exposure. A comparison of Figures 7 and 8a illustrates that although there are significant chemical transformations induced by X-ray irradiation, the total halogen (Cl, F) content within the film remains relatively constant. Similarly, the total C and O areas shown in Figure 8b indicate that the amount of carbon- and oxygen-containing species that desorb during the irradiation process are negligible. This lack of significant desorption is also consistent with the invariance of the Au signal (Figure 8c). A

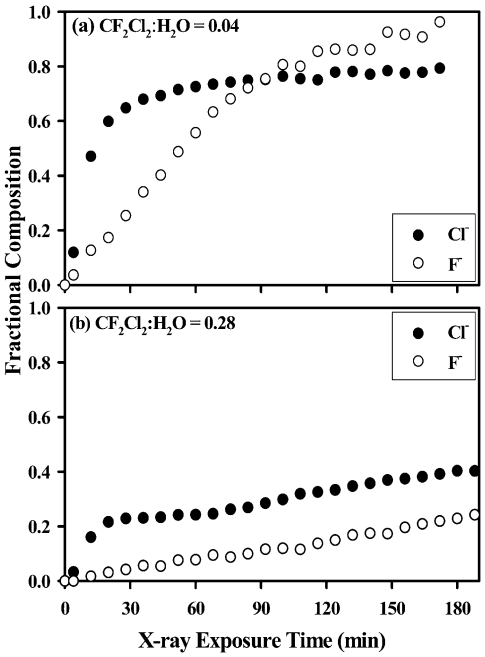

Figure 9. Variation in the Cl^- and F^- production for (a) a dilute film (CF_2Cl_2:$H_2O \approx 0.04$) and (b) an intermediate film (CF_2Cl_2:$H_2O \approx 0.28$) as a function of X-ray exposure time. Cl^- (●) and F^- (○) are represented by their fractional concentrations (see text for details).

similar invariance in the elemental composition of the film was also observed during X-ray irradiation of the CF_2Cl_2/H_2O(ice) film shown in Figure 6.

The fractional concentrations of Cl^- (Cl^-/total Cl area) and F^- ions (F^-/total F area) in CF_2Cl_2/H_2O films illustrated in Figures 6 and 7 as a function of X-ray irradiation time are plotted in Figure 9. Figure 9a shows the variation in the fractional concentration of Cl^- and F^- for the dilute CF_2Cl_2/H_2O film shown in Figure 6 as a function of X-ray exposure. Cl^- production was observed to increase rapidly in the initial stages of irradiation (<30 min) but increased only slowly for longer exposures. In contrast, for the same film, the concentration of F^- ions in the film increased steadily over the time scale of the X-ray irradiation. Figure 9b shows that for the more concentrated CF_2Cl_2/H_2O film shown in Figure 7, the production of Cl^- ions also dominates at short irradiation times (<30 min). However, the fraction of chlorine that is converted to chloride ion is significantly reduced compared to the dilute films (compare Figure 9a,b). In an fashion analogous to that in Figure 9a, the fractional concentration of F^- ions produced in the more concentrated film increased steadily over the course of the experiment although the fractional conversion is reduced.

Figure 10a,b shows the variation in the F 1s and Cl 2p XPS regions following 20 min of X-ray exposure for four films of different initial CF_2Cl_2:H_2O ratios. The F 1s and Cl 2p regions show that the concentration of both F^- and Cl^- ion production is greatest in dilute films. This is shown explicitly in Figure 10c where the fraction of the total Cl and F signal composed of Cl^- and F^- ions after 20 min of X-ray irradiation is presented as a function of the initial CF_2Cl_2:H_2O ratio. This illustrates that the extent of Cl^- and F^- production is dependent upon the initial film composition, with the greatest production in films where the CF_2Cl_2:H_2O ratio is <0.1, decreasing as the CF_2Cl_2:H_2O ratio increases from 0.1 to 0.3. For films with initial CF_2Cl_2:H_2O ratios above 0.3, the fraction of chloride and fluoride anions after 20 min of X-ray exposure was found to be independent of the film's initial CF_2Cl_2:H_2O ratio.

Figure 11 shows the effects of substrate annealing on a CF_2Cl_2 rich film (CF_2Cl_2:$H_2O \approx 0.8$) following 230 min of X-ray irradiation. Figure 11(i) shows the initial C 1s region containing only a single peak at ≈292.5 eV associated with the parent CF_2Cl_2 species. After 230 min of X-ray irradiation, the C 1s region shows that most, if not all, of the CF_2Cl_2 has reacted. A new peak is evident at ≈291 eV, whose peak position is consistent with the presence of either CO_2 or COF_2; in addition, a broad C 1s spectral envelope develops and extends from 293 to 284 eV (Figure 11(ii)). Following X-ray irradiation this film was subsequently heated to increasingly higher substrate temperatures. Figure 11(iii) shows that upon annealing the surface to 220 K (corresponding to a temperature at which CF_2Cl_2, H_2O, CO_2, and COF_2 species are expected to have desorbed), the peak

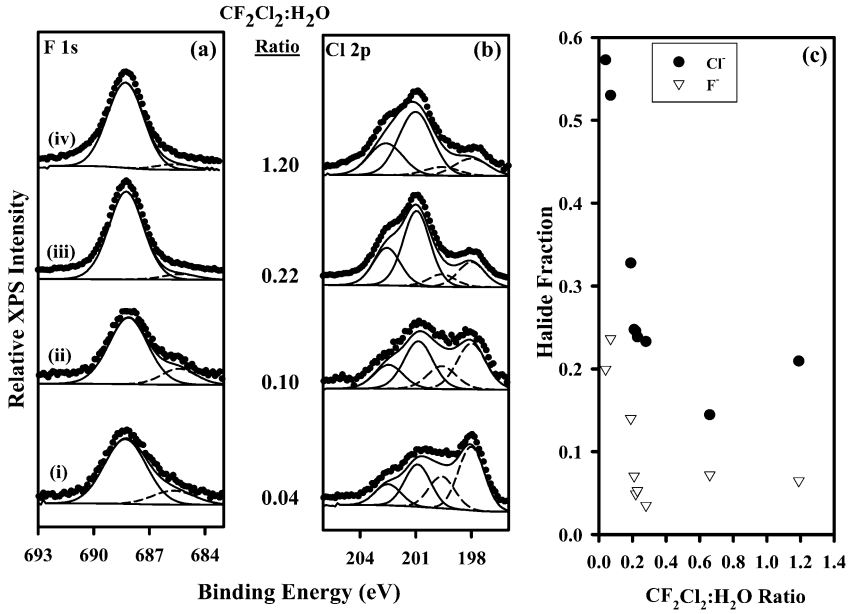

Figure 10. (a) and (b) Variation in the F 1s and Cl 2p XPS regions for a series of different CF_2Cl_2/H_2O ratio films following 20 min of X-ray irradiation: (i) CF_2Cl_2:$H_2O \approx 0.04$; (ii) CF_2Cl_2:$H_2O \approx 0.1$; (iii) CF_2Cl_2:$H_2O \approx 0.22$; (iv) CF_2Cl_2:$H_2O \approx 1.20$. The solid lines in the F 1s and Cl 2p regions correspond to the initial C−F and C−Cl species, and the dotted line correspond to the F^- and Cl^- species. (c) Shows the plot of the Cl^-/Cl_{tot} and F^-/F_{tot} ratios following 20 min of X-ray irradiation as a function of the film's initial CF_2Cl_2:H_2O ratio.

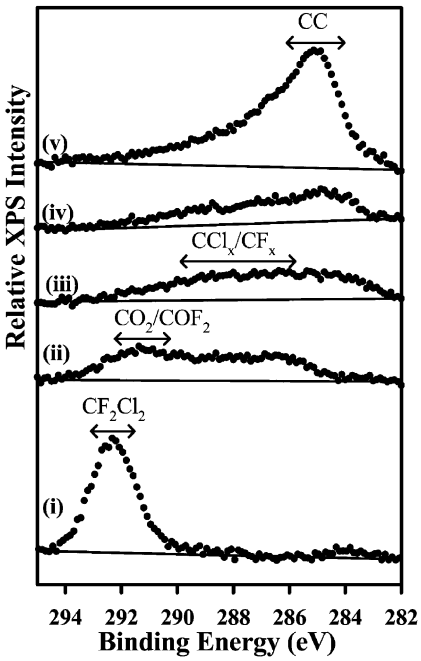

Figure 11. C 1s XPS showing the effect of annealing temperature on an X-ray irradiated CF_2Cl_2/H_2O film (CF_2Cl_2:$H_2O \approx 0.8$): (i) initial film at 100 K; (ii) film after 230 min X-ray irradiation at 100 K and then after subsequent annealing to (iii) 220 K, (iv) 273 K, and (v) 560 K. Spectra (iii)−(v) were taken above 200 K to minimize readsorption of background gases (CO_2, CF_2Cl_2, H_2O).

at 291 eV disappears whereas the broad C 1s envelope extending to lower binding energies remains. Indeed, the C 1s XPS signal remained virtually constant above 200 K until the surface was heated above 500 K when the broad C 1s peak profile was replaced by a dominant peak at 285 eV (compare Figure 11(iv),(v)) assigned to a graphitic overlayer. Measurements in the F 1s and Cl 2p region indicated that changes in the C 1s region upon annealing correlate with the desorption of C−Cl and C−F species evidenced by the loss of C−Cl and C−F species from the Cl 2p and F 1s regions respectively (not shown).

4. Discussion

Structure of Film. The structure and phase of an amorphous solid water (ASW) film is dependent upon the deposition temperature, pressure, and dosing conditions. Extensive experimental[55] and theoretical[60,61] studies indicate that background deposited water at substrate temperatures <120 K gives rise to an amorphous microporous structure, which is metastable with respect to crystalline ice. In contrast, background water deposition above 130 K results in the formation of pore-free solid ice. Generally, there is a correlation between low temperatures and high-deposition fluxes with higher amorphous ice porosity and surface roughness. Monte Carlo ballistic deposition models of background adsorption/desorption processes at ≈100 K predict the formation of an amorphous microporous ice film.[60,61] Kay et al.[62] have studied the influence of dosing conditions upon the ice microstructure using an effusive beam source. In their study, pore-free H_2O films could be grown as low as 22 K if a well-collimated H_2O vapor beam at normal incidence was used for deposition, although at off normal or under background dosing conditions highly porous ice films result from water deposition at 22 K.

In TPD experiments, the substrate temperature was ≈25 K and water was deposited using directional dosing (normal incidence). The same dosing conditions were also employed for co-deposition of CF_2Cl_2 and H_2O. In both cases, we expect a pore free amorphous film. In pure D_2O films (Figure 1(i)) a shoulder is observed within the $m/q = 20$ desorption profile, characteristic of the irreversible phase transition from amorphous to crystalline ice. This shoulder reflects the fact that metastable ASW and crystalline ice have different desorption rates due to the higher free energy of ASW compared to crystalline ice.[47,63] Figure 1(ii) indicates that the water-phase transition persists for a coadsorbed CF_2Cl_2/H_2O(ice) film when the concentration of CF_2Cl_2 molecules in the film is small. The desorption of CF_2Cl_2 from coadsorbed CF_2Cl_2/H_2O(ice) films occurs mainly from two states at ≈110 K and ≈165 K along with a shoulder at ≈170 K. The ≈110 K peak corresponds closely to that measured for CF_2Cl_2 sublimation from a pure CF_2Cl_2 film, whereas desorption from the higher temperature ≈165 K peak coincides with the amorphous/crystalline-phase transition of D_2O (compare Figure 1(ii),(iii)). TPD experiments of films with a similar chemical composition (CF_2Cl_2:$H_2O \approx 0.04$) but different film thicknesses reveal that the number of CF_2Cl_2 molecules desorbing in the lower temperature peak remains constant.[45] In contrast, there is a strong correlation between film thickness and the number of molecules desorbing from the higher temperature peak.

In accord with previous studies of CCl_4 adsorbed on ice films, we attribute the lower temperature (≈110 K) peak to desorption of CF_2Cl_2 from the surface of the microporous ASW ice structure, because the area of this feature is expected to be independent of the film thickness. Additional insight into the nature of the higher temperature CF_2Cl_2 desorption feature can be obtained from recent CCl_4 and ASW studies by Smith et al.[64] In the case of D_2O adsorbed on top of CCl_4, Smith et al. observed a higher temperature CCl_4 peak at ≈161 K coincident with the onset of water crystallization. It was proposed that structural changes that occur in the ASW during crystallization result in defects (cracks, fissures, and/or grain boundaries) that provide "connected" pathways for the CCl_4 to desorb, giving rise to a "molecular volcano" CCl_4 desorption peak. The authors conclude that these results support the idea that the phase transition of ASW is the driving force for CCl_4 desorption. Gentry et al.[65] also studied the influence of ice microstructure on the desorption kinetics of CCl_4 adsorbed on amorphous ice (∼500 ML). For CCl_4 deposited on the ice films grown at ≈95 K (background dosing), the CCl_4 TPD spectra consisted of peaks associated with desorption from micropores that occur at temperatures higher than that for CCl_4 sublimation from the ice surface. They proposed that during the water amorphous to crystalline-phase transition, the higher temperature CCl_4 desorption peak occurs as a result of the crystallization of the amorphous ice surrounding the trapped CCl_4 clusters. The nucleation of crystallites at temperatures near the amorphous/crystalline-phase transition results in the depletion of amorphous ice surrounding CCl_4, providing an escape pathway for the trapped CCl_4. On the basis of these considerations, it is likely that the higher temperature (≈165 K) CF_2Cl_2 peak that coincides with the amorphous/crystalline ice transition observed in our studies is associated with the desorption of CF_2Cl_2 trapped within the amorphous ice matrix. The model of CF_2Cl_2 distributed uniformly throughout the pore free ASW films is also consistent with the fact that the integrated intensity scales with the film thickness. Irrespective of the detailed mechanistic rationale for the higher temperature CF_2Cl_2 peak, Figure 1 indicates that atmospheric species such as CF_2Cl_2 coadsorbed in ice films can exhibit enhanced thermal stability above and beyond that anticipated solely from their bulk thermodynamic properties.

In our XPS and IR experiments, water and CF_2Cl_2 were coadsorbed from the background onto the Au substrate at temperatures of ≈100 K. Under these conditions we anticipate that the film consists of microporous amorphous ice that contains CF_2Cl_2 both at the surface and trapped within the ASW matrix.

X-ray-Induced Reactivity within the CF_2Cl_2/H_2O(Ice) Film. Because the efficiency of direct X-ray-induced photodissociation of molecules in most cases is very low, photogenerated primary and low-energy secondary electrons from the substrate are believed to be largely responsible for the modification process. For example, it has been established that X-ray-induced defluorination in fluorine-containing organic thin films is mediated by low-energy secondary photoelectrons produced by the initial interaction of X-rays with the adsorbate and/or substrate.[58,66] Similarly, the chemical reactions observed in the present study are postulated to involve low-energy secondary electrons generated within the CF_2Cl_2/H_2O(ice) film and from the metallic substrates as a result of X-ray irradiation. This idea is also supported by the observation that low-energy electron-beam irradiation of CF_2Cl_2/H_2O(ice) films also produces CO_2, COF_2, H_3O^+, Cl^-, and F^-.[45]

Low-energy electrons can induce chemical reactions either by ionization, excitation, or resonant electron attachment.[67] In the low-energy range (0−10 eV), dissociative electron attachment (DEA) is believed to be largely responsible for halogen bond cleavage.[9] On the basis of previous gas-phase studies,[9,20] the dominant pathway during DEA of CF_2Cl_2 involves a resonant electron capture at energies <1 eV and involves primarily C−Cl rather than C−F bond cleavage, as indicated in section 1,

$$CF_2Cl_2 + e^- \rightarrow \cdot CF_2Cl + Cl^- \qquad (1)$$

In gas-phase DEA[22] of CF_2Cl_2, Cl^-:F^- ratio yields are ≈10. This gas-phase data is similar to our observation of greater chloride anion yields at low X-ray exposures (Figure 10) and supports the idea that in the condensed CF_2Cl_2-containing films, the initial bond breaking process in CF_2Cl_2 molecules induced by X-ray irradiation also involves DEA mediated C−Cl rather than C−F bond cleavage.

Rate of CF_2Cl_2 Decomposition. X-ray-induced reactions within the CF_2Cl_2/H_2O(ice) films were found to proceed without significant radiation-stimulated desorption (Figure 8). Under these conditions the rate of CF_2Cl_2 loss from the film will be the result of the DEA process (eq 1). Consistent with eq 1, Figure 3 shows that the loss of CF_2Cl_2 in the film, measured by the integrated IR area of the peaks at 1146 and 1090 cm^{-1} as a function of X-ray exposure, can be well fit by a first-order decay curve modified by the nonuniform intensity profile of the X-ray beam (shown by the dashed line).[58] In the context of Figure 3, the nonuniformity of the X-ray source is responsible for the persistent, nonzero CFC signal at longer X-ray exposures. The effect of the film's initial CF_2Cl_2:H_2O ratio on the rate of X-ray-induced CF_2Cl_2 loss is shown in Figure 5. Statistical analysis revealed that for CF_2Cl_2:H_2O ratios <0.3, the difference in the rate of CF_2Cl_2 decomposition is independent of the film's initial chemical composition (inset to Figure 5). Results by Lu and Sanche,[13] however, were interpreted to indicate that the DEA cross-section is enhanced by 10^2 to 10^3 for CFCs adsorbed on polar dielectric media, namely, ammonia and water. They attribute this to electrons of kinetic energies <1 eV that are in precursor states being trapped in a solvent cage. A relative increase in the cross-section for electron-induced decomposition of CF_2Cl_2 (180 eV electrons) was also determined by TPD measurements from the CF_2Cl^+ fragment (m/q = 85) of an electron-irradiated CF_2Cl_2/H_2O/Ru(0001) surface;[45] however, the increase is considerably smaller than that reported by Lu and Sanche.[13] IR results in the present investigation show that within experimental error, the rate of CF_2Cl_2 decomposition under the influence of X-ray irradiation is independent of the film's initial CF_2Cl_2:H_2O ratio for values <0.3. In the context of the likely structure of the CF_2Cl_2/H_2O(ice) film, this suggests that the rate of the initial DEA process is largely independent of the local chemical environment surrounding a CF_2Cl_2 molecule within the film.

SCHEME 1: Proposed Reaction Scheme Showing the Electron-Stimulated Decomposition Pathways for CF_2Cl_2 in CF_2Cl_2/H_2O Films[a]

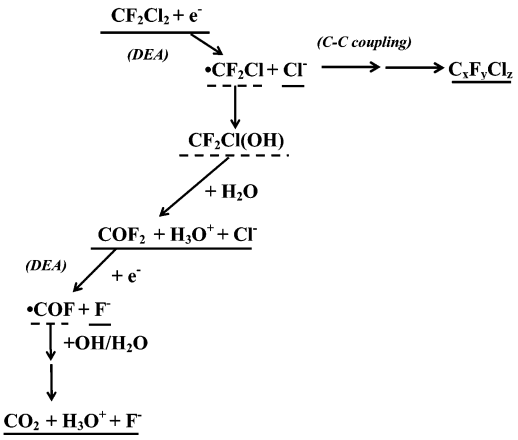

[a] Solid lines indicate stable species that are observed, and dotted lines indicate postulated reactive intermediates.

The principal chemical reactions proposed to be responsible for production of the carbon-containing species observed in this study are shown in Scheme 1. The radiation chemistry of halogenated hydrocarbons in the presence of water is an extremely complicated subject. Despite the complexity of radiation-induced chemistry in water, a number of studies have shown that the dominant reaction products can be described by a small subset of reaction steps. For example, UV photodegradation studies of CCl_4 and $CHCl_3$ in the presence of water show that the production of OH and halomethyl radicals ($\cdot CCl_3$, $\cdot CHCl_2$) are the dominant initial reaction pathways.[68] Scheme 1 represents the dominant reaction pathways that we believe are responsible for the production of COF_2, CO_2, H_3O^+, F^-, and Cl^- as well as the CF_xCl_y species observed for CF_2Cl_2 rich films. In the following sections, specific details of the elementary reaction steps responsible for each of the products observed are presented.

COF_2 Production. The formation of carbonyl difluoride (COF_2) from CF_2Cl_2 is most significant at short X-ray exposures (Figures 2 and 3) and is postulated to occur as a result of reactions associated with the $\cdot CF_2Cl$ intermediate formed in the initial DEA process (eq 1) and hydroxyl radicals, the latter generated by electron-stimulated reactions of H_2O, thus[69]

$$\cdot CF_2Cl + \cdot OH \rightarrow CF_2Cl(OH) \qquad (2a)$$

$$CF_2Cl(OH) \xrightarrow{H_2O} COF_2 + H_3O^+ + Cl^- \qquad (2b)$$

The formation of carbonyl dihalides (COX_2) from CX_4 species (X = halogen) has generally been ascribed to the reaction of hydroxyl radicals and $\cdot CX_3$ intermediates. For example, this process has been invoked to describe the production of COF_2 during the plasma abatement of CHF_3 and CF_4,[70] and $COCl_2$

during electron beam irradiation,[34] sonochemical remediation,[71] and anaerobic photocatalytic hydrolysis[72] of CCl_4.

Another possible reaction pathway involves further DEA of the $\cdot CF_2Cl$ species leading to the production of difluorocarbene ($:CF_2$)[74] whose subsequent reactions with hydroxyl radicals have been predicted to lead to COF_2;[75]

$$\cdot CF_2Cl + e^- \rightarrow :CF_2 + Cl^- \quad (3a)$$

$$:CF_2 + \cdot OH \rightarrow COF_2 + H \quad (3b)$$

However, any $:CF_2$ produced would also be expected to react readily with H_2O molecules in the ice film to produce CO and HF,[76,77] thus

$$:CF_2 + H_2O \rightarrow CO + 2\,HF \quad (4)$$

In the present study, there is no evidence of any CO production, either as a stable molecular species in the film (evidenced by the lack of any IR intensity at 2200 cm^{-1} associated with the C≡O stretch) or as a gas-phase species. In contrast, recent results in our laboratory have revealed the production of methane (evidenced by the appearance of the in-plane deformation mode at 1300 cm^{-1}) trapped in ice films during the electron-stimulated reactions of methyl iodide (CH_3I) coadsorbed in H_2O(ice) films.[73] Because CH_4 and CO should exhibit comparable thermal stability ($\Delta_{sub}H(CO) \approx 6$ kJ mol^{-1}, $\Delta_{sub}H(CH_4) \approx 8$ kJ mol^{-1}),[78] the absence of any IR intensity at ≈2200 cm^{-1} supports the idea that CO is not a significant product of electron-stimulated reactions of CF_2Cl_2 in ice films.

Support for the idea that the difluorocarbene species is not a significant reactive intermediate in the present study is also provided by the absence of any C_2F_4 (evidenced by the lack of 1337 and 1186 cm^{-1} antisymmetric and symmetric ν(CF) IR modes),[79] even in more concentrated CF_2Cl_2 films where the probability of bimolecular coupling is enhanced. In this context it should be noted that previous studies have shown the propensity for difluorocarbene ($:CF_2$) to engage in bimolecular coupling reactions to produce C_2F_4.[80,81] In contrast, during electron beam irradiation of CCl_4/H_2O(ice) films, C_2Cl_4 was routinely observed in CCl_4 rich films due to carbon−carbon coupling reactions associated with the dichlorocarbene ($:CCl_2$) species.[34,35] This is further supported by TPD results of electron-beam irradiated CF_2Cl_2/H_2O and CCl_4/H_2O mixtures where C_2Cl_4 was detected but not C_2F_4. Another experimental observation that supports the idea that the dominant route for COF_2 production is based on the reactivity of $\cdot CF_2Cl$ rather than $:CF_2$ is the fact that the production of COF_2 is correlated with the observation of H_3O^+, consistent with reactions 2a and 2b but inconsistent with 3a and 3b.

Interestingly, we find that COF_2 is the exclusive carbonyl dihalide species produced. There was no evidence for the Fermi resonance doublet ν(CO), ν(CF + CCl), and ν(CF) modes associated with COFCl expected at 1876, 1850, and 1095 cm^{-1}, respectively[79,82] (Figure 2), whose band intensities can reasonably be anticipated to be comparable to that of COF_2. Similarly, there was no IR intensity associated with the production of phosgene ($COCl_2$: $\nu(CO) = 1798$ cm^{-1}). The selectivity toward COF_2 as opposed to either COFCl or $COCl_2$ indicates that the first two carbon−halogen bond-breaking events are dominated by C−Cl rather than C−F cleavage. The absence of $COCl_2$ can readily be explained by the dominance of C−Cl rather than C−F bond breaking during the initial DEA to CF_2Cl_2. The absence of any COFCl production, however, associated with the reactivity of the $\cdot CF_2Cl$ intermediate and the decomposition of $CF_2Cl(OH)$ is postulated to be a consequence of the greater thermodynamic stability of COF_2. Thus, the experimental heat of formation of COF_2 is approximately ≈200 kJ mol^{-1} more exothermic than COFCl, and the greater stability of COF_2 is principally a result of the greater C−F versus C−Cl bond strength.[83]

CO_2 Production. Figure 3 illustrates that COF_2 is not stable to continued X-ray irradiation but behaves as a reactive intermediate, being both produced and destroyed by electron-stimulated processes. The production of CO_2 is postulated to occur as a result of the electron-stimulated degradation of COF_2 (Scheme 1) through a mechanism analogous to the one responsible for COF_2 production from CF_2Cl_2:

$$COF_2 + e^- \rightarrow \cdot COF + F^- \quad (5a)$$

$$\cdot COF + \cdot OH \rightarrow \rightarrow CO_2 + H_3O^+ + F^- \quad (5b)$$

Support for the idea that COF_2 is the reactive precursor for the formation of CO_2 in the present study is provided by Figure 3, which indicates that there is a finite induction period during the initial stages of X-ray irradiation before the appearance of CO_2.

Once produced, CO_2 remains stable within the film. This is supported by the fact that the IR area of CO_2 produced by X-ray irradiation was constant in the absence of X-ray irradiation, indicating the absence of both (i) significant CO_2 adsorption from the background, and (ii) COF_2 hydrolysis to produce CO_2 and HF under these low (≈100 K) temperature conditions. Furthermore, in separate experiments carried out on ice films coadsorbed with CO_2 alone, the integrated CO_2 IR area was invariant to the effect of X-ray irradiation over a period of several hours.

Cl^- and F^- Production in the Film. During the early stages of the reaction, Cl^- ions are the dominant ionic species produced in the film, evidenced by the variation in the Cl 2p and F 1s regions (Figures 6 and 7). This is principally a result of the dominance of C−Cl bond cleavage in both the initial DEA of CF_2Cl_2 (eq 1) and also in the reactions of the $\cdot CF_2Cl$ intermediate (eqs 2a and 2b). In contrast F^- ions are generated primarily as a result of reactions associated with COF_2 (eqs 5a and 5b) and as a result, the initial production of F^- ions lags behind Cl^- ions (Figure 9). Despite the chemical transformations within the Cl 2p and F 1s regions during X-ray irradiation accompanying the formation of Cl^- and F^- ions from C−Cl and C−F species, respectively, the total integrated Cl 2p and F 1s XPS areas remain virtually constant during X-ray irradiation. This indicates that Cl^- and F^- ions are efficiently solvated (trapped) in part because of their low mobility within the ice film under these low-temperature conditions and do not escape into the vacuum. It should also be noted that no evidence for Cl_2 or F_2 formation was observed in this investigation or in related studies on the effect of electron beam irradiation on CF_2Cl_2/H_2O(ice) films.[45]

Carbon−Carbon Coupling Reactions in the Film. In more CF_2Cl_2-rich films XPS measurements indicate that a partially halogenated CCl_xF_y carbonaceous film is produced during X-ray irradiation of CF_2Cl_2/H_2O(ice) films. This is most clearly evidenced by the appearance of a broad C 1s spectral envelope below 290 eV for CF_2Cl_2 rich films, shown in Figure 11, consistent with the presence of a broad distribution of local chemical environments for carbon atoms (e.g., C−Cl, C−F, *C*F−CF). A similar phenomenon was observed previously during the electron beam irradiation of CCl_4-rich CCl_4/H_2O(ice)

films and has been ascribed to carbon−carbon coupling reactions between carbon-containing radical species produced during electron-stimulated reactions.[35] Recent evidence of carbon−carbon coupling reactions has also been observed in the electron-induced reactions of condensed cyclopropane.[84] In that study, propene was identified as the major initial product whose subsequent electron-stimulated reactions produced longer hydrocarbon chains.

The production of polymeric CF_xCl_y during X-ray irradiation of CF_2Cl_2-rich films is also consistent with the evolution of the C 1s region during thermal annealing after X-ray irradiation (Figure 11). Specifically, the broad C 1s envelope remains unchanged between 200 K and ≈500 K well above the temperature where all of the molecular species produced during the X-ray irradiation process (e.g., CO_2 and COF_2) are expected to desorb (<200 K). The idea that the C 1s profile shown in Figure 11(iii) corresponds to a carbon-rich film compared to the initial CF_2Cl_2 adsorbate is supported by the 3:1:1, C:Cl:F ratio of the CF_xCl_y film, calculated from analysis of the C 1s, Cl 2p, and F 1s XPS regions, respectively. Upon further annealing of the CF_xCl_y film to approximately 560 K, thermal dissociation of the C−Cl and C−F bonds occurs to leave behind a predominantly graphitic overlayer, evidenced by the dominance of a single peak at ∼285 eV in the C 1s region (Figure 11(v)). Consistent with this assertion is the absence of any spectral intensity in the Cl 2p or F 1s XPS regions at 560 K. Thermal desorption of chlorine and fluorine also increases the film density and the relative concentration of carbon, resulting in an increased C 1s XPS signal (compare Figure 11(iv),(v)). A similar phenomena has been observed during previous studies on the X-ray-induced degradation of a semi-fluorinated self-assembled monolayer, where the predominance of C−F bond breaking in the film produced a stabilized cross-linked carbonaceous overlayer and a concomitant increase in the C 1s XPS area.[85] It should also be noted that in Scheme 1 carbon−carbon coupling reactions involving the •COF intermediate are also possible, and are probably responsible for the presence of a small amount of oxygen in the CF_xCl_y films, evidenced by the continued presence of XPS intensity associated with oxygen-containing functionality (determined from analysis of the O 1s region) in the film above 200 K. For clarity this process has been omitted from Scheme 1.

Effect of the Film's Initial Chemical Composition on Product Distribution. Differences in the product partitioning as a function of the film's initial chemical composition can largely be correlated with the fate of the $\cdot CF_2Cl$ intermediate produced as a result of the initial C−Cl bond cleavage event (Scheme 1). Thus in dilute films, reactions of the $\cdot CF_2Cl$ intermediate with oxygen-containing species (see previous section) are believed to be correlated with the formation of COF_2 and after prolonged periods of X-ray exposure CO_2 (Figure 3). Indeed, CO_2 is essentially the exclusive carbon-containing species ultimately produced in dilute films where the initial CF_2Cl_2:H_2O(ice) ratio is low (≈1:10). This is indicated by the XPS data shown in Figure 6 that shows that virtually all of the carbon initially present as CF_2Cl_2 (C 1s peak at 291 eV) is ultimately converted into CO_2 (C 1s peak at 291 eV), corroborated by RAIRS results shown in Figures 2−4.

In contrast, during X-ray irradiation of CF_2Cl_2 rich films where the CF_2Cl_2:H_2O ratio is high (≈1:1) carbon-coupling reactions become significant, as evidenced by the production of the partially halogenated CF_xCl_y polymeric film (e.g., Figure 11). The increased probability of carbon−carbon coupling reactions decreases the amount of COF_2 and CO_2 produced in the film (Scheme 1). This is evidenced by the IR results shown in Figure 4, where the concentrations of CO_2 and COF_2 decrease (after a fixed period of X-ray irradiation) with higher initial CF_2Cl_2 concentrations in the film, although the rate of CF_2Cl_2 loss remains constant.

When background dosing conditions are used to generate the CF_2Cl_2/H_2O(ice) films (prevalent for the XPS and RAIRS studies) the initial film is expected to consist of microporous amorphous ice that contains CF_2Cl_2 at the surface and trapped within the ASW matrix. Under the influence of subsequent X-ray irradiation, reactions between oxygen-containing species such as hydroxyl radicals and fragments of CF_2Cl_2 dissociation such as $\cdot CF_2Cl$ are most likely to occur at the interfacial regions that exist between domains of H_2O and CF_2Cl_2 within the amorphous ice matrix. In contrast, carbon−carbon coupling reactions are expected to occur for CF_2Cl_2 molecules initially present as part of a discrete cluster within the film. For these considerations it is clear that CO_2 and COF_2 production will be favored in dilute films where, on average, CF_2Cl_2 molecules are surrounded by a large number of adsorbed H_2O molecules whereas the carbon−carbon coupling process will predominate in more concentrated films, where extensive CF_2Cl_2 clustering within the amorphous film is anticipated.

Figure 4 reveals that over the concentration range studied in the present investigation, there is no significant difference in the rate of CF_2Cl_2 depletion. However, Figure 10 indicates that in more H_2O-rich films, after a fixed period of X-ray irradiation, a greater fraction of Cl and F is converted into Cl^- and F^-. Thus, though Cl^- ions are always generated during the initial DEA process, the production of subsequent halide ions (Cl^- or F^-) is ultimately dependent upon the fate of the $\cdot CF_2Cl$ intermediate. In dilute films, the dominant reaction channels involve the production of Cl^- from direct DEA of CF_2Cl_2 and during COF_2 formation, followed by F^- during CO_2 production (Scheme 1). In contrast, the fate of any carbon-containing radical intermediate in more CF_2Cl_2 rich films is likely to involve carbon−carbon coupling reactions, leading to the production of a CF_xCl_y overlayer. Thus, the greater fraction of chloride/fluoride ions produced in more water rich films (Figure 10) after a fixed period of X-ray irradiation is the result of the production of "solvated" Cl^- and F^- ions. The continued production of Cl^- and F^- ions in films that possess a high initial concentration of CF_2Cl_2 (Figure 9b) for prolonged periods of X-ray irradiation is ascribed to electron-stimulated C−Cl and C−F bond cleavage within the polymeric CF_xCl_y films formed in these more concentrated films.

There has been lively discussion in the literature[16−19] concerning the potential atmospheric significance of radiation-induced processes involving CF_2Cl_2 at ice surfaces. Under stratospheric conditions ($T \approx 200$ K) there is a dynamic equilibrium between CF_2Cl_2 adsorption and desorption onto PSCs. The concentration of CF_2Cl_2 in the stratosphere is $\sim 10^{13}$ molecule/cm^3, and under these conditions, the steady-state surface density of CF_2Cl_2 has been estimated to be $\sim 10^{11}$ molecule/cm^2.[11] Despite the approximations inherent in this calculation, the results indicate that CF_2Cl_2 molecules are present in trace concentrations on the surface of PSCs; consequently, electron-stimulated reactions of CF_2Cl_2/H_2O(ice) films may play a contributing role in determining the fate of CF_2Cl_2 in the stratosphere. Various forms of high-energy radiation such as cosmic rays can liberate low-energy secondary electrons during irradiation of PSCs. Under atmospheric conditions where the CF_2Cl_2:H_2O ratio for CF_2Cl_2 molecules adsorbed on the surface of or in PSCs is low (<0.1), the dominant products arising from

the interaction of these low-energy secondary electrons with CF_2Cl_2/H_2O(ice) films are expected to be COF_2 and CO_2, F^-, Cl^-, and H_3O^+. Thus, the interaction of high-energy radiation with CF_2Cl_2 will therefore contribute to the budget of COF_2 and CO_2, two important atmospheric species. In this context, it should be noted that COF_2 is the third largest source of fluorine in the atmosphere[86] and its UV photolysis leads to the production of fluorine atoms that can contribute to the catalytic cycle associated with stratospheric ozone depletion.

5. Conclusions

The interaction of X-ray irradiation with amorphous CF_2Cl_2/H_2O(ice) films generates a cascade of low-energy electrons. The dominant initial radiation-induced process in adsorbed CF_2Cl_2 is C−Cl bond cleavage via dissociative electron attachment (DEA), producing $\cdot CF_2Cl$ and Cl^-, the latter effectively solvated within the ice film. Although no strong dependence on the rate of X-ray-induced CF_2Cl_2 depletion was observed, the product partitioning was strongly influenced by the film's initial CF_2Cl_2:H_2O ratio. In dilute films (CF_2Cl_2:$H_2O < 0.1$) DEA to produce solvated Cl^-, followed by reactions between the $\cdot CF_2Cl$ intermediate and oxygen-containing species are postulated to be responsible for the exclusive production of the most thermodynamically stable carbonyl dihalide (COF_2) along with hydroxonium ions (H_3O^+) and Cl^- anions. Upon continued X-ray irradiation, carbonyl difluoride undergoes further electron-stimulated decomposition to yield CO_2 as the stable final carbon-containing species in the film in the absence of any significant contribution from electron-stimulated desorption. CO_2 production is also accompanied by the formation of hydroxonium and fluoride anions. In films more concentrated with CF_2Cl_2 molecules, however, carbon coupling reactions between carbon-containing radicals become important, leading to the production of a partially halogenated polymeric carbonaceous overlayer that remains stable until C−Cl and C−F bond cleavage occurs above 500 K to leave a residual graphitic overlayer.

Acknowledgment. Support for this research was provided by the National Science Foundation (No. CHE-0089168) as part of the Collaborative Research Activities in Environmental Molecular Science in Environmental Redox-Mediated Dehalogenation Chemistry at Johns Hopkins University. T.E.M. also acknowledges support at Rutgers University from the National Science Foundation, Grant CHE 0075995.

References and Notes

(1) Solomon, S. *Rev. Geophys.* **1999**, *37*, 275.
(2) Molina, M. J.; Rowland, F. S. *Nature* **1974**, *249*, 810.
(3) McCormack, J. P.; Steele, H. M.; Hamill, P.; Chu, W. P.; Swissler, T. J. *J. Atmos. Sci.* **1982**, *39*, 1387.
(4) Hall, E. J. *Radiation and Life*; Pergamon Press: New York, 1984.
(5) Madey, T. E.; Johnson, R. E.; Orlando, T. M. *Surf. Sci.* **2002**, *500*, 838.
(6) Sanche, L. *Surf. Sci.* **2000**, *451*, 82.
(7) Akbulut, M.; Sack, N. J.; Madey, T. E. *Surf. Sci. Rep.* **1997**, *28*, 177.
(8) Schulz, G. J. *Rev. Mod. Phys.* **1973**, *45*, 423.
(9) Illenberger, E.; Scheunemann, H. U.; Baumgaertel, H. *Chem. Phys.* **1979**, *37*, 21.
(10) Wayne, R. P. *Chemistry of Atmospheres*; Clarendon Press: Oxford, U.K., 1985; Chapter 6.
(11) Lu, Q.-B.; Madey, T. E. *J. Chem. Phys.* **1999**, *111*, 2861.
(12) Lu, Q.-B.; Madey, T. E. *Surf. Sci.* **2000**, *451*, 238.
(13) Lu, Q.-B.; Sanche, L. *Phys. Rev. B* **2001**, *63*, 153403.
(14) Lu, Q.-B.; Madey, T. E. *J. Phys. Chem. B* **2001**, *105*, 2779.
(15) Lu, Q.-B.; Sanche, L. *Phys. Rev. Lett.* **2001**, *87*, 078501.
(16) Harris, N. R. P.; Farman, J. C.; Fahey, D. W. *Phys. Rev. Lett.* **2002**, *89*, 219801.
(17) Lu, Q.-B.; Sanche, L. *Phys. Rev. Lett.* **2002**, *89*, 219802.
(18) Patra, P. K.; Santhanam, M. S. *Phys. Rev. Lett.* **2002**, *89*, 219803.
(19) Lu, Q.-B.; Sanche, L. *Phys. Rev. Lett.* **2002**, *89*, 219804.
(20) Ingolfsson, O.; Weik, F.; Illenberger, E. *Int. J. Mass. Spectrom. Ion Processes* **1996**, *155*, 1.
(21) Kiendler, A.; Matejcik, S.; Skalny, J. D.; Stamatovic, A.; Maerk, T. D. *J. Phys. B* **1996**, *29*, 6217.
(22) Christophorou, L. G.; Olthoff, J. K.; Wang, Y. *J. Phys. Chem. Ref. Data* **1997**, *26*, 1205.
(23) *Atmospheric chemistry and global change*; Brasseur, G. P., Orlando, J. J., Tyndall, G. S., Eds.; Oxford University Press: New York, 1999; Chapter 8.
(24) Mak, F. T.; Zele, S. R.; Cooper, W. J.; Kurucz, C. N.; Waite, T. D.; Nickelsen, M. G. *Water Res.* **1997**, *31*, 219.
(25) Orlando, T. M.; Kimmel, G. A.; Simpson, W. C. *Nucl. Instrum. Methods Phys. Res. B* **1999**, *157*, 183.
(26) Sieger, M. T.; Simpson, W. C.; Orlando, T. M. *Nature* **1998**, *394*, 554.
(27) Kimmel, G. A.; Orlando, T. M.; Vezina, C.; Sanche, L. *J. Chem. Phys.* **1994**, *101*, 3282.
(28) Kimmel, G. A.; Orlando, T. M. *Phys. Rev. Lett.* **1995**, *75*, 2606.
(29) Kimmel, G. A.; Tonkyn, R. G.; Orlando, T. M. *Nucl. Instrum. Methods Phys. Res. B* **1995**, *101*, 179.
(30) Kimmel, G. A.; Orlando, T. M. *Phys. Rev. Lett.* **1996**, *77*, 3983.
(31) Kimmel, G. A.; Orlando, T. M.; Cloutier, P.; Sanche, L. *J. Phys. Chem. B* **1997**, *101*, 6301.
(32) Noell, J. O.; Melius, C. F.; Stulen, R. H. *Surf. Sci.* **1985**, *115*, 119.
(33) Simpson, W. C.; Parenteau, L.; Smith, R. S.; Sanche, L.; Orlando, T. M. *Surf. Sci.* **1997**, *390*, 86.
(34) Wagner, A. J.; Vecitis, C.; Fairbrother, D. H. *J. Phys. Chem. B* **2002**, *106*, 4432.
(35) Wagner, A. J.; Vecitis, C.; Wolfe, G. M.; Perry, C. C.; Fairbrother, D. H. *Phys. Chem. Chem. Phys.* **2002**, *4*, 3806.
(36) Tobien, T.; Cooper, W. J.; Nickelsen, M. G.; Pernas, E.; O'Shea, K. E.; Asmus, K.-D. *Environ. Sci. Technol.* **2000**, *34*, 1286.
(37) Evans, D.; Rosocha, L. A.; Anderson, G. K.; Coogan, J. J.; Kushner, M. J. *J. Appl. Phys.* **1993**, *74*, 5378.
(38) Ding, W.; McCorkle, D. L.; Pinnaduwage, L. A. *J. Appl. Phys.* **1998**, *84*, 3051.
(39) Torres, J.; Perry, C. C.; Bransfield, S. J.; Fairbrother, D. H. *J. Phys. Chem. B* **2002**, *106*, 6265.
(40) Carlo, S. R.; Torres, J.; Fairbrother, D. H. *J. Phys. Chem. B* **2001**, *105*, 6148.
(41) Faradzhev, N. S.; Kusmierek, D. O.; Yakshinskiy, B. V.; Solovev, S.; Madey, T. E. *Surf. Sci.* **2003**, *528*, 20.
(42) *The Handbook of X-ray Photoelectron Spectroscopy*; Muilenberg, G. E., Ed.; Perkin-Elmer Corp.: 1979.
(43) AugerScan, 2.4 ed.; RBD Enterprises Inc.
(44) Emfietzoglou, D.; Moscovitch, M. *Nucl. Instrum. Methods Phys. Res. B* **2002**, *193*, 71.
(45) Faradzhev, N. S.; Perry, C. C.; Kusmierek, D. O.; Fairbrother, D. H.; Madey, T. E. Manuscript in preparation.
(46) Thiel, P. A.; Madey, T. E. *Surf. Sci. Rep.* **1987**, *7*, 211.
(47) Speedy, R. J.; Debenedetti, P. G.; Smith, R. S.; Huang, C.; Kay, B. D. *J. Phys. Chem.* **1996**, *100*, 240.
(48) Banham, S. F.; Sodeau, J. R.; Horn, A. B.; McCoustra, M. R. S.; Chesters, M. A. *J. Vac. Sci. Technol. A* **1996**, *14*, 1620.
(49) Barone, S. B.; Zondlo, M. A.; Tolbert, M. A. *J. Phys. Chem. A* **1999**, *103*, 9717.
(50) Schaff, J. E.; Roberts, J. T. *Langmuir* **1999**, *15*, 7232.
(51) Shimanouchi, T. *J. Phys. Chem. Ref. Data* **1977**, *6*, 993.
(52) Giorgianni, S.; Gambi, A.; Franco, L.; Ghersetti, S. *J. Mol. Spectrosc.* **1979**, *75*, 389.
(53) Mallinson, P. D.; McKean, D. C.; Holloway, J. H.; Oxton, I. A. *Spectrochim. Acta Part A−Mol. Biomol. Spectrosc.* **1975**, *A31*, 143.
(54) Stolov, A. A.; Herrebout, W. A.; van der Veken, B. J. *J. Mol. Struct.* **1999**, *481*, 499.
(55) Delzeit, L.; Rowland, B.; Devlin, J. P. *J. Phys. Chem.* **1993**, *97*, 10312.
(56) Barone, S. B.; Zondlo, M. A.; Tolbert, M. A. *J. Phys. Chem. B* **1999**, *103*, 9717.
(57) Carlo, S. R.; Grassian, V. H. *J. Phys. Chem. B* **2000**, *104*, 86.
(58) Graham, R. L.; Bain, C. D.; Biebuyck, H. A.; Laibinis, P. E.; Whitesides, G. M. *J. Phys. Chem.* **1993**, *97*, 9456.
(59) Perry, C. C.; Wagner, A. J.; Fairbrother, D. H. *Chem. Phys.* **2002**, *280*, 111.
(60) Zhdanov, V. P.; Norton, P. R. *Surf. Sci.* **2000**, *449*, L228.
(61) Zhdanov, V. P.; Norton, P. R. *Surf. Sci.* **2000**, *459*, 245.
(62) Stevenson, K. P.; Kimmel, G. A.; Dohnálek, Z.; Smith, R. S.; Kay, B. D. *Science* **1999**, *283*, 1505.
(63) Blanchard, J. L.; Roberts, J. T. *Langmuir* **1994**, *10*, 3303.
(64) Smith, R. S.; Huang, C.; Wong, E. K. L.; Kay, B. D. *Phys. Rev. Lett.* **1997**, *79*, 909.

(65) Sadtchenko, V.; Knutsen, K.; Giese, C. F.; Gentry, W. R. *J. Phys. Chem. B* **2000**, *104*, 2511.
(66) Laibnis, P. E.; Graham, R. L.; Biebuyck, H. A.; Whitesides, G. M. *Science* **1991**, *254*, 981.
(67) Sanche, L. *J. Phys. B: At. Mol. Opt. Phys.* **1990**, *23*, 1597.
(68) Shirayama, H.; Toshezo, Y.; Taguchi, S. *Water Res.* **2001**, *35*, 1941.
(69) Balkas, T. I.; Fendler, J. H.; Schuler, R. H. *J. Phys. Chem.* **1971**, 455.
(70) Wofford, B. A.; Jackson, M. W.; Hartz, C.; Bevan, J. W. *Environ. Sci. Technol.* **1999**, *33*, 1892.
(71) Hua, I.; Hoffmann, M. R. *Environ. Sci. Technol.* **1996**, *30*, 864.
(72) Calza, P.; Minero, C.; Pelizzetti, E. *Environ. Sci. Technol.* **1997**, *31*, 2198.
(73) Perry, C. C.; Wagner, A. J.; Wolfe, G.; Torres, J.; Fairbrother, D. H.; Farazhev, N. S.; Madey, T. E. Manuscript in preparation.
(74) Rebbert, R. E.; Ausloos, P. J. *J. Photochem.* **1975**, *4*, 419.
(75) Liu, R.; Francisco, J. S. *J. Phys. Chem. A* **1998**, *102*, 9869.
(76) Francisco, J. S. *J. Phys. Chem.* **1989**, *93*, 8118.
(77) Francisco, J. S.; Goldstein, A. N.; Li, Z.; Zhao, Y.; Williams, I. H. *J. Phys. Chem.* **1990**, *94*, 4791.
(78) *CRC Handbook of Chemistry and Physics*, 75th ed.; Lide, D. R., Ed.; CRC Press Inc.: Boca Raton, FL, 1994.
(79) Shimanouchi, T. *Tables of Molecular Vibrational Frequencies Consolidated Volume I*; National Bureau of Standards: Washington, DC, 1972; p 1.
(80) Jensen, M. B.; Thiel, P. A. *J. Am. Chem. Soc.* **1995**, *117*, 438.
(81) Hou, Y.-C.; Chao-Ming-Chiang. *J. Am. Chem. Soc.* **1999**, *121*, 8116.
(82) Bouteiller, Y.; Abdelaoui, O.; Schriver, A.; Schriver-Mazzuoli, L. *J. Chem. Phys.* **1995**, *102*, 1731.
(83) Chase, M. W., Jr. *J. Phys. Chem. Ref. Data* **1998**, *9*, 1.
(84) Swiderek, P.; Deschamps, M. C.; Michaud, M.; Sanche, L. *J. Phys. Chem. B* **2003**, *107*, 563.
(85) Wagner, A. J.; Carlo, S. R.; Vecitis, C.; Fairbrother, D. H. *Langmuir* **2002**, *18*, 1542.
(86) Raper, D. F.; Farmer, C. B.; Zander, Z.; Park, J. H. *J. Geophys. Res.* **1987**, *92*, 9851.